



AIAA 2003-5114

**Mean Flow Approximation for a Slab
Rocket Motor with Tapered Sidewalls**

O. C. Sams, IV and J. Majdalani
Marquette University
Milwaukee, WI 53233

Propulsion Conference and Exhibit
20–23 July 2003
Huntsville, AL

Mean Flow Approximation for a Slab Rocket Motor with Tapered Sidewalls

Oliver C. Sams, IV* and Joseph Majdalani†
Marquette University, Milwaukee, WI 53233

and

Gary A. Flandro‡
University of Tennessee Space Institute, Tullahoma, TN 37388

Internal flowfield modeling is a requisite for obtaining critical parameters for the design of modern solid rocket motors. In this study, the analytical development of internal flowfields particular to solid rocket motors with tapered sidewalls is pursued. The analysis employs the vorticity-stream function approach to treat this problem assuming steady, incompressible, inviscid and non-reactive flow conditions. The resulting solution is rotational and inviscid following the analyses presented by Culick for a cylindrical solid rocket motor. In an extension to Culick's classic work, Clayton has recently managed to incorporate the effect of small wall taper. A similar approach to that of Clayton will be applied to the slab motor in which the chamber will be modeled as a rectangular channel with porous, tapered sidewalls. The current solution will be shown to be reducible, at leading order, to Taylor's inviscid profile in a channel with transpiring walls. The analysis also captures the generation of vorticity at the surface of the propellant and its transport along the streamlines due to axial pressure gradients. It is from the axial pressure gradients that the proper form of the vorticity is ascertained. Throughout, the method of regular perturbations is used to solve the nonlinear vorticity equation that governs the tapered flow. To further understand the effects of the taper, comparisons of total pressure and velocity profiles in tapered and non-tapered chambers are entertained. This study constitutes a small step in improving our current modeling capabilities of internal flows in chambers with variable cross section.

Nomenclature

A	= surface area
A_0	= minimum cross sectional area
h_0	= chamber half height
L_0	= length of non-tapered segment
L	= normalized chamber length, L_0 / h_0
p	= normalized pressure, $p^* / (\rho v_b^2)$
$\bar{u}(x)$	= normalized average velocity, $\bar{u}^*(x) / v_b$
u_b	= injection velocity along the burning surface
u	= normalized axial velocity, u^* / v_b
v	= normalized transverse velocity, v^* / v_b
w_0	= chamber width
x	= normalized distance from the head end of the tapered segment, x^* / h_0

y	= normalized transverse coordinate, y^* / h_0
y_s	= distance to tapered surface measured from the midsection plane
α	= taper angle
β	= ratio of maximum to average velocity at a given cross section, $u_{\max} / \bar{u}(x)$
β_0	= constant, $\frac{1}{2} \pi$
ε	= perturbation parameter, $\sin(\alpha)$
Ω_s	= surface vorticity
Ω	= mean flow vorticity, $\Omega^* h_0 / v_b$
ψ_s	= stream function along the surface
ψ	= stream function, $\psi^* / (v_b h_0)$

Subscripts

0	= entrance conditions; leading order
1	= of first order
s	= slanted coordinate along tapered surface
b	= burning surface conditions
\max	= maximum value

Superscript

$*$	= dimensional quantity
-----	------------------------

*Graduate student and Research Associate, Department of Mechanical and Industrial Engineering. Member AIAA.

†Assistant Professor, Department of Mechanical and Industrial Engineering. Member AIAA.

‡Boling Chair Professor of Excellence in Propulsion, Department of Mechanical and Aerospace Engineering. Associate Fellow AIAA.

I. Introduction

IN the design of solid rocket motors, internal flowfield modeling is of paramount importance in evaluating the impact of mean flow on unsteady wave motions, estimating acoustic energy, predicting the onset of hydrodynamic instability, and assessing velocity and pressure coupling with propellant burning. Naturally, accurate mathematical modeling of the pressure distribution and velocity profiles are important with respect to the efficient design and manufacture of the structural components that comprise the rocket motor.

If the pressure load is over-predicted, the result is increased motor cost and weight; this can have a negative effect on motor efficiency. If the pressure load is under-predicted, the risk is motor failure. In 1966, Culick¹ developed a mean flow solution for the internal flowfield of a circular-port motor using an inviscid, incompressible and rotational flow model. This profile was used in many studies to predict the pressure variation and combustion instabilities. In fact, it has often been used as a baseline in known ballistic codes such as SSPP (Standard Stability Prediction Program).

Modern solid rocket motors are manufactured with small tapered angles that reduce the contact between the casting mandrels and the propellant to facilitate their removal. The small, divergent angles aid in the reduction of shear stress on the surface of the propellant, thereby minimizing the likelihood of propellant tearing, cracking and/or debonding. The tapers are also used to shape the thrust time curve and to soften thrust transients at tail-off.²

The problem is that most ballistic codes used to assess the physical characteristics of solid rocket motors do not account for the small tapered angles presently found in modern solid rocket motors. The issue here is that when the code utilizes Culick's or Taylor's profiles to evaluate tapered solid rocket motors, the pressure drop may be over-predicted. In an effort to produce a solution that yields the proper pressure correction applicable to tapered walls, Clayton was able to obtain an approximate solution by employing a regular perturbation method. Being asymptotic, Clayton's solution was shown to be reducible, at leading order, to Culick's profile for a taper angle of zero.

In 1956, Taylor³ derived the solution for a rectangular chamber with porous walls as part of his treatment of pressure-driven flows in wedges and cones. Other pertinent solutions were later advanced by Yuan and Finkelstein⁴ and Terrill^{5,6} who incorporated the effects of viscosity in both axisymmetric and planar domains. Their work was recently extended to include the effects of wall regression by Majdalani, Vyas and Flandro,⁷ and Zhou and Majdalani.⁸

The physical model to be considered here combines the flow in a porous channel with that in a porous channel with tapered sidewalls. The importance of taper in the context of internal flow studies of rocket motors seems to have been overlooked in the literature. In fact, one may find very few studies concerned with tapered chambers. One such study may be attributed to the work of Mu-Kuan and Tong-Miin.⁹ In their attempt to understand the flowfield present in tapered ducts applicable to solid propellants, Mu-Kuan and Tong-Miin⁹ conducted a fiber optic study of a non-uniform, injection induced flow in tapered channels. The principal focus of their study was to determine the effect of the divergent configuration on the promotion of flow stability. Their study also confirmed the lack of similarity between the velocity distributions in straight (non-tapered) and tapered chambers.

The study here is intended to contrast mean velocity distributions and compare the pressure drop between the two geometries. It will also address the mathematical peculiarities connected with the no slip condition along the tapered surface.

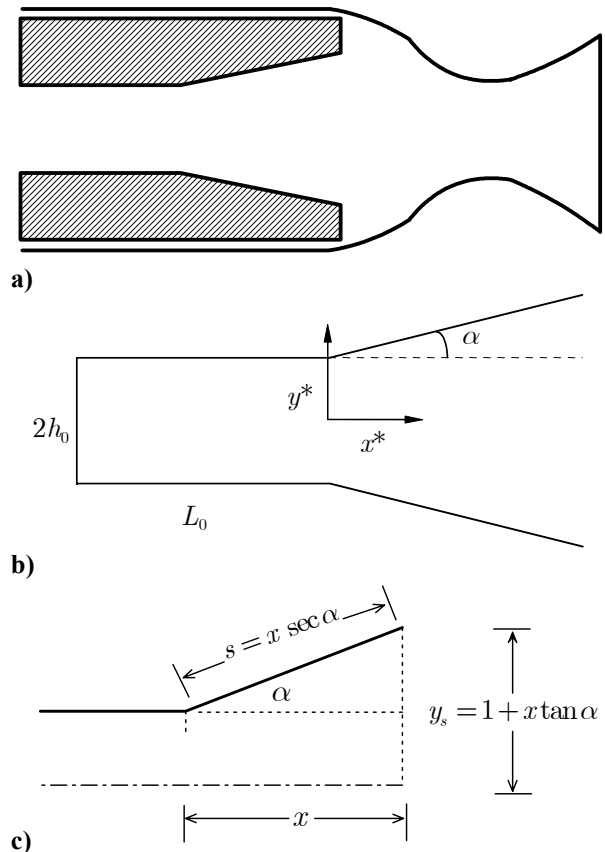


Fig. 1 Sketches depicting a) a typical motor with taper, b) the dimensional reference frame, and c) the normalized surface coordinates.

II. Methodology

To begin the analysis, the velocity will be formulated as a function of the axial coordinate x^* . Next, the axisymmetric stream function and axial pressure gradient are developed using the known physical quantities along the tapered surface. The significance of the pressure gradient and surface vorticity allow the proper form of the chamber vorticity to be ascertained; this results in a non-linear governing partial differential equation. The surface vorticity is then written in terms of the stream function. Finally, the resulting equation is solved using a perturbation expansion.

The key aspect of the solution lies, perhaps, in expressing the vorticity as function of the stream function along the surface. Then knowing that both the vorticity and stream functions do not change along a streamline, the vorticity evolution along a streamline is captured throughout the chamber.

The problem concerns the two-dimensional flow within a rectangular channel of half height h_0 , width w_0 , and a tapered angle α . Here we use Cartesian coordinates, where x^* is the dimensional axial coordinate and y^* is the dimensional transverse coordinate (see Fig. 1b). The mathematical model is based on the rotational form of the momentum equation for incompressible, inviscid and steady fluid.

The tapered slab geometry is based on the Cartesian coordinate system where x^* is the dimensional axial coordinate and y^* is the dimensional transverse coordinate. The area of the tapered surface is given by

$$A_b = w_0 x^* \sec \alpha \quad (1)$$

The chamber's cross sectional area may be evaluated from

$$A(x^*) = w_0 (h_0 + x^* \tan \alpha) \quad (2)$$

The inflow cross-sectional area at the interface of the tapered and straight portion of the chamber is clearly

$$A_0 = w_0 h_0 \quad (3)$$

The corresponding velocity becomes

$$u_0^* = (L_0 / h_0) v_b \quad (4)$$

Normalizing the entrance velocity with the injection velocity v_b and the chamber half height h_0 , Eq. (4) becomes

$$u_0 = L \quad (5)$$

Here L can be defined as the bulk flow parameter because it is directly proportional to the average velocity at the entrance to the tapered portion. Due to mass conservation, the cross sectional average velocity

of the fluid at any axial location x^* may be expressed by

$$\bar{u}^*(x^*) = \frac{A_0 u_0^* + A_b u_b}{A(x^*)} \quad (6)$$

By substituting Eqs. (1), (2) and (3) into equation (6) and normalizing with v_b and h_0 , one gets

$$\bar{u}(x) = \frac{L + x \sec \alpha}{1 + x \tan \alpha} \quad (7)$$

The stream functions are used to satisfy the continuity equation. The axial and transverse velocities are related to the stream function as usual via

$$u^* = \frac{\partial \psi^*}{\partial y^*}, \quad v^* = -\frac{\partial \psi^*}{\partial x^*} \quad (8)$$

The stream function along the boundary can be evaluated after finding the directional derivative along the simulated burning surface. Using the chain rule, one can put

$$\frac{d\psi_s}{ds} = \frac{\partial \psi_s}{\partial x} \cos \alpha + \frac{\partial \psi_s}{\partial y_s} \sin \alpha \quad (9)$$

where $\psi = \psi^* / (v_b h_0)$. Along the surface (see Fig. 1c), these variables can be expressed by

$$x = s \cos \alpha \quad (10)$$

$$y_s = 1 + x \tan \alpha \quad (11)$$

$$u_s = u(x, y_s) = \sin \alpha \quad (12)$$

$$v_s = v(x, y_s) = -\cos \alpha \quad (13)$$

The normalized definitions for the axial and transverse velocities are substituted to get

$$\frac{d\psi_s}{ds} = v_s \cos \alpha + u_s \sin \alpha \quad (14)$$

The stream function can now be determined along the tapered wall by substituting Eqs. (12) and (13) into Eq. (14) and integrating along the surface; one finds

$$\frac{d\psi_s}{ds} = \cos^2 \alpha + \sin^2 \alpha = 1 \quad (15)$$

Integrating and applying the boundary condition necessary to express the velocity in terms of the stream function, it is clear that

$$\psi_s = s + L \quad (16)$$

In terms of x , Eq. (16) becomes

$$\psi_s = x \sec \alpha + L \quad (17)$$

By substituting Eqs. (17) and (11) into Eq. (7), the average velocity can be expressed in terms of the stream function and the slanted coordinate along the tapered surface. One finds

$$\bar{u}(x) = \psi_s / y_s \quad (18)$$

where y_s is the distance from the axis to the tapered surface as expressed in the relationship

$$y_s = 1 + x \tan \alpha \quad (19)$$

The axial pressure gradient is obtained using Bernoulli's equation along a streamline situated in the midsection plane. Consequently, one obtains

$$p(x) = p_0 - \frac{1}{2} u_{\max}^2(x) \quad (20)$$

The total pressure in the combustion chamber of solid rocket motors is sensitive to the shape of the axial profiles. In non-tapered chambers, the shape of the axial profile is determined by the ratio of the axial velocity to the axial distance. In accordance with the no slip condition, this ratio must be a constant equal to $\pi/2$. For diverging ducts, the axial profile is changing as the gases move downstream; it is required that the shape of the profile be known at each axial location in order to obtain accurate pressure estimates. Considering that the maximum velocity is unknown, it is expedient to define a ratio between the maximum and average local velocities at any axial location x . This velocity ratio can be written as

$$\beta(x) = \frac{u_{\max}(x)}{\bar{u}(x)} \quad (21)$$

The form of $\beta(x)$ will be determined later as needed to satisfy the no slip demand along the tapered surface. By substituting Eq. (21) into Eq. (20), one can put

$$p(x) = p_0 - \frac{1}{2} \beta^2 \bar{u}^2(x) \quad (22)$$

The pressure gradient can be determined along the surface by calculating the derivative of Eq. (22), as shown in Eq. (23). The result is

$$\frac{dp(x)}{dx} = -\beta^2(x) \bar{u}(x) \left[\frac{d\bar{u}(x)}{dx} + \frac{\bar{u}(x)}{\beta(x)} \frac{d\beta(x)}{dx} \right] \quad (23)$$

Differentiating Eq. (18) yields

$$\frac{d\bar{u}}{dx} = \frac{\sec \alpha}{y_s} - \frac{\psi_s \tan \alpha}{y_s^2} \quad (24)$$

By substituting Eq. (24) into Eq. (23) and simplifying, it follows that

$$\frac{dp}{dx} = -\frac{\beta^2 \psi_s \sec \alpha}{y_s^2} \left[1 - \frac{\psi_s \tan \alpha}{y_s} + \psi_s \cos \alpha \left(\frac{\beta'}{\beta} \right) \right] \quad (25)$$

where

$$\beta' = d\beta / dx \quad (26)$$

Vorticity is produced at the surface as a result of the interaction between the injected fluid and the axial pressure gradient. This phenomenon can be depicted in the momentum equation for steady inviscid flows viz.

$$\mathbf{u}^* \times \boldsymbol{\Omega}^* = \nabla \left(p^* / \rho + \frac{1}{2} \mathbf{u}^* \cdot \mathbf{u}^* \right) \quad (27)$$

Normalizing and evaluating Eq. (27) at the surface gives

$$\Omega_s = -\frac{dp}{ds} \quad (28)$$

where s is the slanted coordinate along the tapered surface situated at an angle α . This choice is convenient given the fact that the vorticity is transported along the streamlines. In terms of the stream function, it can be expressed as

$$-\Omega(x, y) = \frac{\partial^2 \psi}{\partial x^2} + \frac{\partial^2 \psi}{\partial y^2} \quad (29)$$

The surface vorticity is obtained from Eq. (28) and is readily expressed in terms of the pressure gradient along the surface; this can be accomplished by putting

$$\Omega_s = -\frac{dp}{ds} = -\frac{\partial p}{\partial x} \cos \alpha - \frac{\partial p}{\partial y_s} \sin \alpha \quad (30)$$

Since the pressure variation in the transverse direction is known to be negligibly small, Eq. (30) reduces to

$$\Omega_s = -\frac{dp}{dx} \cos \alpha + O(\sin \alpha) \quad (31)$$

Substitution of Eq. (25) into Eq. (31) yields the following relationship for the stream function and surface vorticity

$$\Omega_s = -\frac{\beta^2 \psi_s}{y_s^2} \left[1 - \frac{\psi_s \sin \alpha}{y_s} + \psi_s \cos \alpha \left(\frac{\beta'}{\beta} \right) \right] \quad (32)$$

Since the vorticity is transported along the streamlines (see Fig. 2), it is convenient to express the distance from the axis to the injection plane in terms of the stream function. Combining Eqs. (17) and (19) produces

$$y_s = 1 + (\psi_s - L) \sin(\alpha) \quad (33)$$

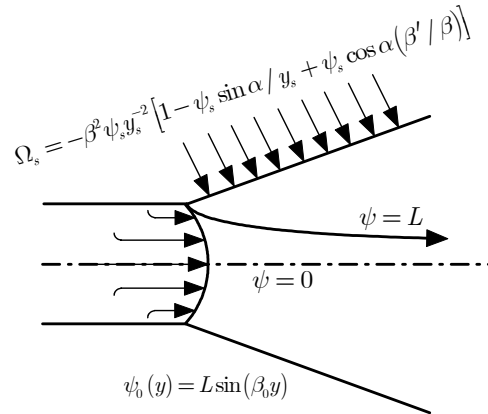


Fig. 2 Mathematical model

From Eqs. (32) and (33), the vorticity at any point in the chamber can be determined. For streamlines originating in the straight (non-tapered) portion of the chamber, the vorticity can be expressed as

$$\Omega(\psi, y) = -\beta^2 \psi \quad (34)$$

The chamber vorticity in the tapered region is described by Eq. (32). Combining Eqs. (29) and (32) furnishes the governing equation for the tapered slab geometry. One finds

$$\frac{\partial^2 \psi}{\partial x^2} + \frac{\partial^2 \psi}{\partial y^2} = -\frac{\beta^2 \psi}{y_s^2} \left[1 - \frac{\psi \sin \alpha}{y_s} + \psi \cos \alpha \left(\frac{\beta'}{\beta} \right) \right] \quad (35)$$

For axisymmetric flow, the boundary conditions required to solve Eq. (35) are

$$\psi(x, 0) = 0 \quad (36)$$

and, along the tapered surface,

$$\psi(x, y_s) = \psi_s \quad (37)$$

III. Solution

For the cylindrical case, Clayton² determined the relative magnitudes of the axial derivatives of the stream function and the velocity ratio by numerical analysis. Based on his results, Clayton was able to deduce that the axial derivatives were negligibly small.² In particular, Clayton noted that β' and $\partial^2 \psi / \partial x^2$ were small quantities. Clayton's observations may be verified using a scaling analysis. Considering that

$$\frac{\partial^2 \psi}{\partial x^2} = \frac{\partial v}{\partial x} \quad (38)$$

one may recall that v is independent of x in the straight channel, thus causing Eq. (38) to vanish. Evidently, the presence of small taper will not affect the size of this term. In essence, it is postulated that the axial derivatives are so small that they can be neglected in the prescribed tapered domain. Once the proper form the velocity ratio has been obtained, a scaling analysis will be employed once more to further justify neglecting β' . Equation (35) can hence be reduced into

$$\frac{\partial^2 \psi}{\partial y^2} = -\frac{\beta^2 \psi}{y_s^2} \left(1 - \frac{\psi \sin \alpha}{y_s} \right) \quad (39)$$

Since the reduced equation is non-linear, a solution can now be sought by the method of regular perturbations. Accordingly, the stream function and velocities are expanded in the form

$$\psi = \psi_0 + \psi_1 \varepsilon + O(\varepsilon^2) \quad (40)$$

$$u_s = u_{s0} + u_{s1} \varepsilon + O(\varepsilon^2) \quad (41)$$

Similarly, by expanding Eq. (21), one obtains

$$\beta_s = \beta_0 + \psi_s \beta_1 \varepsilon + O(\varepsilon^2) \quad (42)$$

where the perturbation parameter is due to the small taper angle, namely,

$$\varepsilon = \sin(\alpha) \quad (43)$$

The governing equation can be solved by first inserting Eq. (33) into Eq. (39), and then expanding in the form of Eq. (40). The method of regular perturbations linearizes the governing equation, making a solution by standard methods accessible.

A. Leading Order Solution

At the leading order (ε^0), one obtains

$$\frac{d^2 \psi_0}{dy^2} + \frac{\beta_0^2 \psi_0}{y_s^2} = 0 \quad (44)$$

This is a second order, linear differential equation that allows for the simple extraction of the transverse variation of the stream function. The general solution can be expressed as

$$\psi_0(y) = C_1 \cos(\beta_0 y / y_s) + C_2 \sin(\beta_0 y / y_s) \quad (45)$$

Now that an amenable form has been obtained, evaluation of Eq. (45) at the conditions provided by Eqs. (36) and (37) produces the first order solution

$$\psi_0(y) = [x \sec(\alpha) + L] \sin(\beta_0 y / y_s) \quad (46)$$

where

$$\beta_0 = \frac{1}{2} \pi \quad (47)$$

It should be noted that at $L = \alpha = 0$, one recovers

$$\psi_0(y) = x \sin(\beta_0 y) \quad (48)$$

Equation (48) represents Taylor's profile for porous flow in channels. The leading order solution, as expressed by Eq. (46), can be described as a stretched version of the Taylor profile. Such a form can be attributed to the additional bulk flow resulting from increased surface area caused by the physical presence of taper.

B. First Order Solution

At first order, the perturbation expansion yields

$$\frac{d^2 \psi_1}{dy^2} + \frac{\beta_0^2 \psi_1}{y_s^2} + \frac{2\beta_0 \beta_1 \psi_0}{y_s^2} - \frac{\beta_0^2 \psi_0^2}{y_s^3} = 0 \quad (49)$$

The first order boundary conditions are

$$\psi_1(0) = 0, \quad \psi_1(y_s) = 0 \quad (50)$$

By application of these boundary conditions, one obtains a first order correction of the form

$$\psi_1(x, y) = \frac{[x \sec(\alpha) + L]^2}{6y_s} \left[3 - 4 \cos\left(\frac{\beta_0 y}{y_s}\right) \right]$$

$$+ \cos\left(\frac{2\beta_0 y}{y_s}\right) - 2 \sin\left(\frac{\beta_0 y}{y_s}\right) + 6y\beta_1 \cos\left(\frac{\beta_0 y}{y_s}\right) \quad (51)$$

Observing Eq. (51), it can be seen that there exists an unknown term that originates from the perturbed velocity ratio β . The final step in the solution process involves solving for the first order velocity ratio β_1 , such that the no-slip condition is satisfied along the tapered surface. Therefore, it is necessary to express the surface velocity using

$$u_s = u_s \cos(\alpha) - v_s \sin(\alpha) = u_{s0} + u_{s1}\varepsilon \quad (52)$$

and so,

$$u_s = \frac{\partial\psi}{\partial y} \cos(\alpha) + \frac{\partial\psi}{\partial x} \sin(\alpha) \\ = (\psi_0 + \psi_1\varepsilon)_y \cos(\alpha) + (\psi_0 + \psi_1\varepsilon)_x \sin(\alpha) \quad (53)$$

Considering that ψ_0 already satisfies the no slip condition at the wall, one may segregate the first order correction by putting

$$u_{s1} = \frac{\partial\psi_1}{\partial y} \cos(\alpha) + \frac{\partial\psi_1}{\partial x} \sin(\alpha) \quad (54)$$

Again, it can be seen that the term containing $\sin(\alpha)$ is negligibly small, being of $O(\varepsilon)$. Setting Eq. (54) equal to zero and evaluating the resulting expression at the tapered surface, one obtains

$$\beta_1 = \frac{2}{3y_s} \quad (55)$$

The required forms of the leading and first order velocity ratios, β_0 and β_1 , have been determined. At this point, it is necessary to make use of a scaling analysis to justify ignoring their derivatives. Expressing Eq. (42) in the form of its derivative, one can put

$$\beta'_s = \beta'_0 + \psi'_s \beta'_1 \varepsilon + O(\varepsilon^2) \quad (56)$$

Then using the known values of the velocity ratios, it follows that

$$\beta'_s = \frac{2}{3} \sin \alpha \left(\psi_s / y_s\right)' \quad (57)$$

Computing the derivative, one obtains

$$\beta'_s = -\frac{2}{3} \sin^2 \alpha \cos^{-2} \alpha (1 + x \tan \alpha)^{-2} = O(\varepsilon^2) \quad (58)$$

Being of $O(\varepsilon^2)$, retaining this term in the first order equation was clearly unnecessary.

C. Velocity, Vorticity and Pressure Relations

Now that the proper form of the stream function has been ascertained, it is possible to extract other useful physical quantities particular to tapered flowfields. A sufficient analysis of the remaining flow

attributes can be made from the leading order solution due to the fact that it recovers the physical characteristics of the taper without the addition of the first order correction. Although the distance to the tapered surface is a function of the axial coordinate x , it is treated as a constant in the evaluation of the velocity, pressure, and vorticity. This is justified by computing the derivatives and observing that the extra terms that arise from the axial variation of the tapered surface are of order $\sin(\alpha)$. Since these terms are of first order, they can be neglected. This enables us to express the desired quantities in a compact and concise form emanating from the leading order solution. Moving on, one can compute the velocity components from the definition of the stream function given by Eq. (8). The axial velocity component may be written as

$$u = \frac{1}{2} \pi \cos(\beta_0 y / y_s) (x \sec \alpha + L) / y_s + O(\varepsilon) \quad (59)$$

and the transverse velocity component may be read from

$$v = -\sec(\alpha) \sin(\beta_0 y / y_s) + O(\varepsilon) \quad (60)$$

Having formulated the velocity field, the pressure gradients can be deduced. In order to obtain the required pressure drop along the chamber, one only needs to integrate the inviscid momentum equations, namely

$$-\frac{\partial p}{\partial x} = u \frac{\partial u}{\partial x} + v \frac{\partial u}{\partial y} \quad (61)$$

$$-\frac{\partial p}{\partial y} = u \frac{\partial v}{\partial x} + v \frac{\partial v}{\partial y} \quad (62)$$

Inserting the axial and transverse velocity relations into Eqs. (61) and (62) yields

$$-\frac{\partial p}{\partial x} = \frac{\pi^2 [x \sec(\alpha) + L]^2}{4y_s^2} \quad (63)$$

$$-\frac{\partial p}{\partial y} = \frac{\pi \sec^2(\alpha)}{4y_s^2} \sin\left(\frac{2\beta_0 y}{y_s}\right) \quad (64)$$

By integrating and combining Eqs. (63) and (64) one is able to produce the spatial variation of the pressure that satisfies both momentum equations. Moving forward, the total pressure can be expressed as

$$-p(x, y) = \frac{1}{8} \pi^2 [x \sec(\alpha) + L]^2 y_s^{-2} \\ + \frac{1}{2} \sec^2(\alpha) \cos^2(\beta_0 y / y_s) + \text{const.} \quad (65)$$

Applying the chamber head end boundary condition, $p(0, 0) = p_0$, one gets

$$p(x, y) - p_0 = -\left\{ \frac{1}{8} \pi^2 [x \sec(\alpha) + L]^2 y_s^{-2} \right. \\ \left. + \frac{1}{2} \sec^2(\alpha) \cos^2(\beta_0 y / y_s) \right\} \quad (66)$$

Using $\Delta p = p(x, y) - p_0$, one can express the pressure drop in the chamber in the following compact form

$$\Delta p = - \left\{ \frac{\pi^2 [x \sec(\alpha) + L]^2}{8y_s^2} + \frac{1}{2} \sec^2(\alpha) \cos^2 \left(\frac{\beta_0 y}{y_s} \right) \right\} \quad (67)$$

In addition to the formulation of the velocity and pressure gradients, one may compute the vorticity in order to complete the extraction of most physical parameters regarding the development of the flowfield. In this respect, the vorticity field can be obtained using

$$\Omega(x, y) = \frac{\partial v}{\partial x} - \frac{\partial u}{\partial y} \quad (68)$$

Inserting the solutions for the velocity components into Eq. (68) produces the expression for the spatial variation of chamber vorticity. One may conclude that

$$\Omega(x, y) = \frac{1}{4} \pi^2 \sin(\beta_0 y / y_s) [x \sec(\alpha) + L] / y_s \quad (69)$$

Each of the required flowfield characteristics particular to tapered slab burners is now at hand. Although mathematical similarities exist between flow in tapered and straight chambers, this does not necessarily account for the physical implications of the present model. Since the tapered angle is known to be small, it should follow that the mean flow characteristics possess minimal variance with the taper angle α . Since this is the case, then one must invoke another parameter that arises from this study. This parameter can be described as the bulk flow parameter $L = u_0$; it is also known as the normalized chamber length $L = L_0 / h_0$. The bulk flow parameter enables us to look at the physical characteristics of small to moderate size motors with tapers. Furthermore, the incorporation of this parameter will make apparent the discrepancies in using non-tapered profiles such as Taylor's to analyze and predict pressure drops and combustion instabilities within rocket motors with tapered sidewalls.

IV. Discussion

A. Streamlines

In order to visualize the motion of the gas in the tapered region several streamlines are plotted for two values of L and the taper angle α . By observing these figures, it can be seen that the taper angle does not have as much effect on the streamlines as does the bulk flow parameter. The bulk flow entering the tapered region emanates from the straight portion of the chamber. The bulk fluid motion can be regulated by varying L or u_0 . Larger values of L correspond to moderate motor sizes and sets the stage for quasi developed flow entering the tapered region (Fig. 3a). Evidently, motors of substantial size (such as the one depicted in Fig. 3b) provide a more developed flow entering the tapered region. In moderate sized tapered solid rocket motors, the gases that are injected from the burning surface into the tapered region are forced to turn quickly as to satisfy continuity. The presence of the bulk flow slows the transverse penetration of the injected gas. For the case of $L = 0$, there is no bulk flow entering the tapered region. As a consequence, the gases can penetrate deeper into the chamber before turning. In comparison to the Taylor profile, the streamlines for this case show weak sensitivity to the angle α .

B. Velocity

Further discussion of the results alludes to the analysis of the axial and transverse velocity profiles. Figure 4a shows the variation of the axial velocity with the transverse coordinate for several values of L and x at constant α . The axial velocity profile changes uniformly as the gases move down the tapered portion of the chamber. Considering the bulk flow parameter, L , which also accounts for the mass flow originating in the straight portion of the chamber, one can come to the conclusion that the axial velocity profile is strongly dependent on the size of the motor. This result can be verified by inspection of Eq. (59).

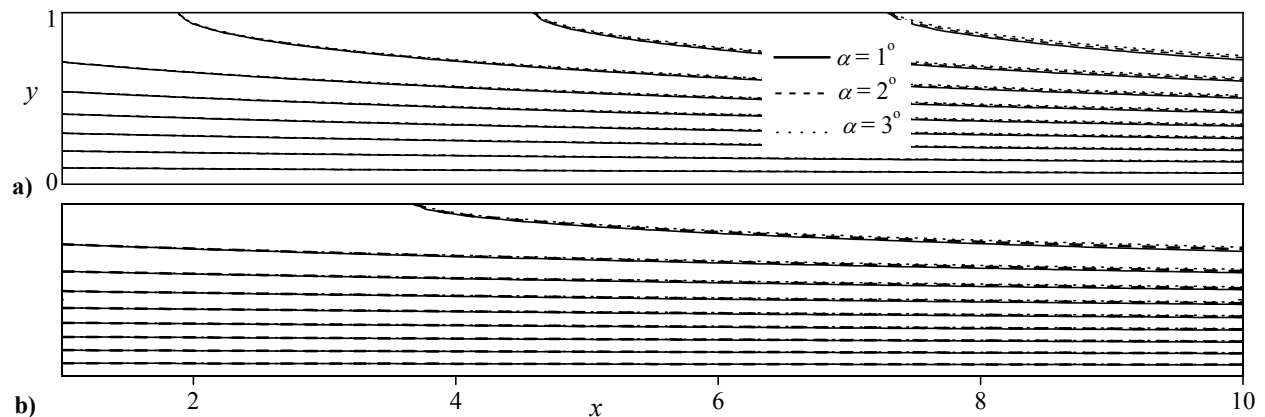


Fig. 3 Streamlines shown for two bulk flow parameters corresponding to a) $L = 2$ and b) $L = 6$.

The larger the straight portion of the motor, the larger the bulk flow emanating from that region. It must be born in mind that the shape of the axial velocity profile depends on the value of β at each axial location. A concurrent investigation of varying taper angles with several axial locations shows, in a descript manner, that the shape must adjust itself at each axial location to fulfill the no slip condition along the tapered surface. This feature of flow in tapered ducts introduces a flat, compact velocity profile in comparison to the Taylor profile.³ In Fig. 4b, the transverse velocity is plotted at distinct values of α including the case of $\alpha = 0$ corresponding to Taylor's profile. The transverse velocity closely mimics the behavior of the profile extracted from Taylor's result. It becomes more linear with increasing taper.

C. Vorticity

Vorticity that is generated along the transpiring surface due to the axial pressure gradient is convected downstream along the streamlines. Vorticity along the simulated burning surface is at its maximum; it decays to zero at the midsection plane. Figure 5 depicts the vortical behavior at a typical taper angle of three degrees for various values of the bulk flow parameter and axial location. For motors with small L , it takes longer for the vorticity to reach its zero value at the midsection-plane. It can also be seen that the axial variation of the vorticity is highly pronounced along the

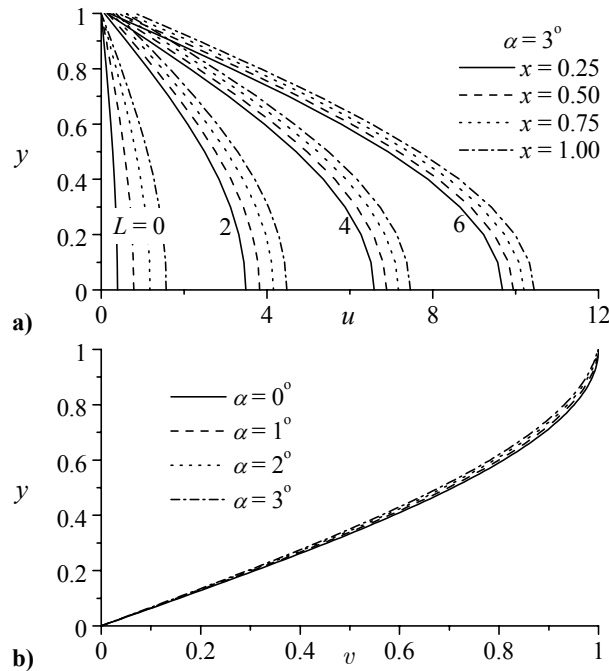


Fig. 4 Characteristic plots of a) axial and b) transverse velocities.

surface. For large bulk flow parameters, vorticity becomes less dependent on the axial position. This can be attributed to the larger contribution of mean flow vorticity emanating from the non-tapered segment.

D. Pressure

As seen in Fig. 6, it is clear that there is a pressure variation with the taper angle that can be even noticed at $x = 1$. As usual the bulk flow parameter L seems to influence the pressure drop in the tapered segment. The slow increase in cross sectional area in the axial direction acts to decrease the pressure drop by allowing a slight build up in local static pressure.

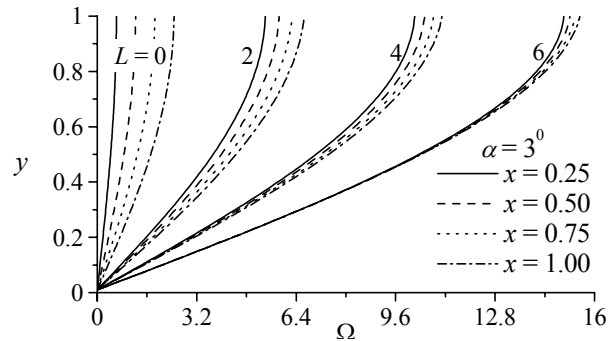


Fig. 5 Vorticity at several axial stations and for increasing bulk flow parameter L .

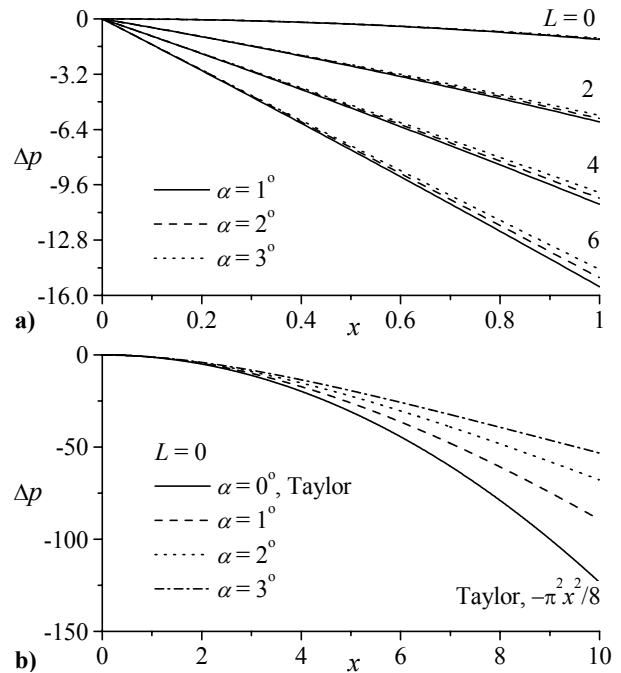


Fig. 6 Pressure drop shown in a) at several values of the bulk flow parameter L . In b) the influence of taper is examined at $L = 0$ and compared to Taylor's injection-driven channel flow with no taper.

As it can be inferred from Fig. 6a, larger motors are seen to exhibit a higher sensitivity to small increases in wall taper. Even in chambers with zero bulk flow, one can extrapolate from Fig. 6b that the influence of minute variations in wall taper can have significant impact on the overall pressure drop. By comparison to Taylor's solution in a straight porous channel, Fig. 6b illustrates the dramatic decreases in the absolute pressure drop at higher taper angles taken at $x = 10$.

In a tapered motor for which the actual pressure drop down the bore is 100 psi, modeling without account for the small taper correction will over-predict the pressure drop to 120 psi or more, depending on the taper angle. Naturally, these differences become larger in longer chambers. The error in predicting the pressure drop without accounting for wall taper increases along the midsection plane of the chamber. As the gases approach the aft end of the motor, the pressure drop can be over-predicted by as much as 50% at larger taper angles. Thus, one can conclude that the incorporation of taper in internal flow analyses is necessary to prevent over-prediction of pressure drop. The taper correction may be particularly important in the manufacture of fail-safe motor casings where precision in pressure estimates is highly desired.

V. Concluding Remarks

A mean flow approximation for flow in solid rocket motors with tapered sidewalls is presented here. In the case for which a tapered channel is compared to its straight counterpart, significant differences are found especially in elongated chambers and in composite chambers consisting of a sizeable straight segment followed by a tapered segment. Some ballistic codes are known to over-predict the pressure drop by applying the straight porous channel solution over the entire chamber length. The corrected solution with taper is suggested here to obtain more accurate estimates of critical parameters needed for efficient motor design and manufacture. The current study may help in fulfilling the need for a model that accounts for a complexly shaped chamber consisting of successive tapered segments. As a baseline case, this model may be applied to the evaluation, estimation, and analysis of hydrodynamic stability and acoustic energy in simulated combustion chambers. In future work, it is hoped that higher order refinements be incorporated into the solution to account for viscous losses and wall regression.

Acknowledgments

The first two authors wish to acknowledge the support received from NASA and the Wisconsin Space Grant Consortium. We are also grateful for the help and assistance received from Curtis D. Clayton at Lockheed Martin. Were it not for his input, this work would not have been possible.

References

- ¹Culick, F. E. C., "Rotational Axisymmetric Mean Flow and Damping of Acoustic Waves in a Solid Propellant Rocket," *AIAA Journal*, Vol. 4, No. 8, 1966, pp. 1462-1464.
- ²Clayton, C. D., "Flowfields in Solid Rocket Motors with Tapered Bores," AIAA Paper 962643, July 1996.
- ³Taylor, G. I., "Fluid Flow in Regions Bounded by Porous Surfaces," *Proceedings of the Royal Society, London, Series A*, Vol. 234, No. 1199, 1956, pp. 456-475.
- ⁴Yuan, S. W., and Finkelstein, A. B., "Laminar Pipe Flow with Injection and Suction through a Porous Wall," *Transactions of the American Society of Mechanical Engineers: Journal of Applied Mechanics, Series E*, Vol. 78, No. 3, 1956, pp. 719-724.
- ⁵Terrill, R. M., "Laminar Flow in a Uniformly Porous Channel with Large Injection," *The Aeronautical Quarterly*, Vol. 16, 1965, pp. 323-332.
- ⁶Terrill, R. M., and Shrestha, G. M., "Laminar Flow through Channels with Porous Walls and with an Applied Transverse Magnetic Field," *Applied Scientific Research*, Vol. 11, 1964, pp. 134-144.
- ⁷Majdalani, J., Vyas, A. B., and Flandro, G. A., "Higher Mean-Flow Approximation for a Solid Rocket Motor with Radially Regressing Walls," *AIAA Journal*, Vol. 40, No. 9, 2002, pp. 1780-1788.
- ⁸Zhou, C., and Majdalani, J., "Improved Mean Flow Solution for Slab Rocket Motors with Regressing Walls," *Journal of Propulsion and Power*, Vol. 18, No. 3, 2002, pp. 703-711.
- ⁹Mu-Kuan, T., and Tong-Miin, L., "Fiber Optic LDV Study of the Non-Uniform, Injection Induced Flow in a 2-D, Divergent, Porous-Walled Channel," *Journal of the Chinese Society of Mechanical Engineers*, Vol. 11, No. 5, 1990, pp. 414-422.